Image Analysis in Light Sheet Fluorescence Microscopy Images of Transgenic Zebrafish Vascular Development

Elisabeth Kugler [1,2] ✉, Timothy Chico [1,2] and Paul Armitage [1]

1 University of Sheffield, Faculty of Medicine, Department of Infection, Immunity and Cardiovascular Disease, S10 2TN Sheffield, United Kingdom.
2 University of Sheffield, The Bateson Centre, Firth Court, Western Bank, Sheffield, S10 2TN United Kingdom.
✉ ekugler1@sheffield.ac.uk

Abstract. The zebrafish has become an established model to study vascular development and disease *in vivo*. However, despite it now being possible to acquire high-resolution data with state-of-the-art fluorescence microscopy, such as lightsheet microscopy, most data interpretation in pre-clinical neurovascular research relies on visual subjective judgement, rather than objective quantification. Therefore, we describe the development of an image analysis workflow towards the quantification and description of zebrafish neurovascular development. In this paper we focus on data acquisition by lightsheet fluorescence microscopy, data properties, image pre-processing, and vasculature segmentation, and propose future work to derive quantifications of zebrafish neurovasculature development.

Keywords: 3D, analysis, development, *in vivo*, light sheet fluorescence microscopy (LSFM), segmentation, vasculature, zebrafish

1 Zebrafish as a Preclinical Model in Cardiovascular Research

The zebrafish embryo is increasingly used to study developmental mechanisms, due to characteristics such as high fecundity, larval transparency and availability of a range of sophisticated experimental approaches [1]. Zebrafish are also becoming a prominent *in vivo* model of cardiovascular development, physiology and pathology [2]. Two main processes, vasculogenesis and angiogenesis, are required to establish the vascular system. Vasculogenesis is *de novo* formation of a basic vascular system via the migration and differentiation of progenitors, called haemangioblasts [3], while angiogenesis describes remodelling and refinement from existing vessels throughout an organisms lifespan [4, 5]. In a pathological context, these processes are associated with chronic inflammatory diseases, vasculopathies or stroke [6] as well as cancer growth, progression and metastasis [7].

1.1 Image Acquisition of the Cardiovascular System in Zebrafish

Labour-intensive microangiography was replaced as the standard visualization technique by the advent of vascular-specific transgenic zebrafish lines (Fig. 1A) [8, 9]. In these transgenic lines, fluorescent reporter genes are expressed in the endothelial cells that line all blood vessels [10]. Thus, imaging these transgenics visualizes the vessel walls, rather than the blood itself, leading to a distinct intensity distribution compared to microangiography or most clinical imaging modalities (Fig. 1B).

Fluorescence microscopy has evolved towards higher image acquisition speed, better resolution and minimization of imaging artefacts [11]. This methodological advancement is typified by state-of-the-art image acquisition methodologies such as lightsheet fluorescence microscopy (LSFM) in which an uncoupling of the microscope illumination and detection paths lead to optical sectioning of samples [12, 13]. This, allows high-speed acquisition with deep tissue penetration and minimal photo-bleaching [14, 15].

The downside of these rapid technical developments are increased data size and complexity, which are computationally challenging to handle. Other challenges, to the quantification of images acquired by LSFM include imaging artefacts, such as the system impulse function (point-spread-function) [16], noise [17], background [18] or refractive index mismatching [19]. Shadowing or stationary periodic noise artefacts can interfere with image quality [20]. Moreover, during *in vivo* imaging motion artefacts can occur due to cardiac pulsation, muscular contraction or microscope focal drift, which are particularly problematic during image acquisitions with lower sampling speed or longer time-lapse. Addressing these technical challenges to answer specific scientific questions is currently beyond the scope of commercially available image analysis software, leading to a diversity of customized software tools for image processing in zebrafish [21]. The majority of developed methods are applied on a whole organism scale in the context of behavioural analysis, phenotype assessment, or tracking to answer questions in the scientific fields of development, morphogenesis, immunology, or toxicology screening.

1.2 Quantitative Analysis of the Vascular System in Zebrafish

Image analysis methodological development for vascular research is mainly driven by clinical imaging. In contrast, objective 3D quantification of *in vivo* vascular development in zebrafish has so far received little attention.

Three-dimenstional analytical and modelling approaches in zebrafish trunk vasculature, based on images acquired by confocal microscopy from microangiography were proposed by Feng et al. [24–26]. They developed a relational-tubular deformable model [25] and statistical assembled deformable model [26] that rely on tubular structures, with axis and surface deformation based on active contour model energy terms. However, the models were only applied to the trunk vasculature and no attempt was made to characterise the cardiovascular system further.

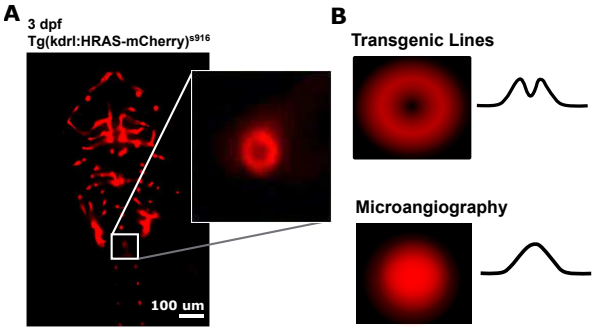

Fig. 1. (A) A variety of transgenic fluorescent reporter lines, such as *tg(kdrl:HRAS-mCherry)^{s916}* [22, 23], can be used to visualize the zebrafish cardiovascular system. **(B)** Vasculature-specific transgenic lines visualize endothelial cells, which encompass the vascular lumen, rather than the blood as is the case in microangiography.

Chen et al. performed the only study to our knowledge addressing 3D zebrafish neurovascular quantification using transgenic lines (visualized with confocal microscopy) [27]. This quantified vessel length, hierarchy, number, loops, as well as pruning events. The method used commercial software (Neurolucida, MicroBrightField, Inc.), but provided little detail about pre-processing, skeletonization, definition of branching points or inscription of expanding spheres, to derive vessel diameters. Another limitation of this study, besides lack of sufficient documentation, is that vessel segment estimations were based on the Euclidean distance along vessel points, which is likely to underestimate the vascular length in high curvature regions, which are common in the dorsal cranial vasculature of embryonic zebrafish.

None of these studies delivered comprehensive global segmentation, allowing representation and/or quantification of different vascular beds. Moreover, the rich data provided by recent imaging methodologies introduces new challenges, as discussed previously. Lastly, to our knowledge, no work has characterised the degree of anatomical conservation or variability within the zebrafish vasculature during development, which would be essential for the assessment of pathological vascular phenotypes.

This scarcity of relevant research is likely due to the following: **(i)** High quality microscope hardware suitable for imaging the zebrafish vasculature system in 3D is a relatively new development. **(ii)** Zebrafish are, in comparison to other preclinical models, still less well adopted in medical sciences. **(iii)** Vessel geometry and topology are subject to intra- as well as inter-object variability [28].

2 Material and Methods

2.1 Zebrafish Husbandry

All experiments were conducted in accordance with institutional and UK Home Office regulations. Maintenance of adult transgenic zebrafish *tg(fli1a:eGFP)*^{y1} [29], *tg(kdrl:HRAS-mCherry)*^{s916} [22, 23], and *tg(fli1a:Lifeact-mClover)*^{sh467} [30] was conducted according to previously described husbandry standard protocols [31], with embryonic staging according to Kimmel et al. [32].

2.2 Image Acquisition

Data acquisition in the dorsal cranial vasculature at 3-4 days post fertilization (dpf) was performed by lightsheet microscope Zeiss Z.1 (software black edition), Plan-Apochromat 20x/1.0 Corr nd=1.38 objective, dual-side illumination with online fusion and activated Pivot Scan at 28 ℃ chamber incubation. Images were obtained with 16bit image depth, 0.334 μm x 0.334 μm x 0.69 μm voxel size resolution, 1920x1920 px (x,y) field of view, and user-defined z-stack depth (typically 400-600 slices). 80 second (sec) with 27 cycles and 10 minute (min) with 200 cycles time-lapse acquisitions were performed with 3 second time intervals. Sample embedding was conducted using 2%-LM agarose (Sigma-Aldrich) in E3 with 0.01 % tricaine (MS-222, Sigma-Aldrich). A dataset with controlled decrease of vascular contrast-to-noise ratio (CNR) was produced in 4dpf *tg(kdrl:HRAS-mCherry)*^{s916} [22, 23] using image acquisition settings as above, but decreasing laser power (LP) with 1.2%, 0.8%, and 0.4%.

2.3 Data Analysis

All image analysis, pre-processing and segmentation were performed using the open-source software Fiji [33].

Image Pre-Processing Sample motion occurring during image acquisition was corrected in original data using the Linear Stack Alignment with Scale Invariant Feature Transform (SIFT) Plugin, implemented in Fiji [33]. The algorithm was run with the following parameters: 1.6px Gaussian blur, 5 steps per scale octave, 30px minimum image size, 1920x1920px single plane field of view, 8 feature descriptors, 0.98 closest/next ratio, 3px maximum alignment error (global alignment with 10px), 0.05 inlier ratio, rigid transform and without interpolation.

Image artefact and noise reduction was performed post motion correction slice-by-slice using a 2D median filter with a radius of 6 voxels (13-by-13 neighbourhood) to remove local noise peaks and valleys [34] and a rolling ball algorithm of size 200 to suppress larger-scale background fluctuations such as scattering, autofluorescence, or shadowing artefacts [35, 17]. These filters were assessed and optimized using intensity measurements of basal artery (BA) cross-sections obtained using the Fiji line ROI [33].

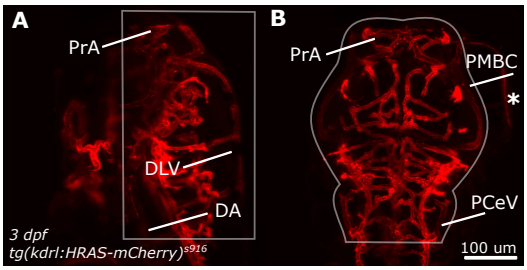

Fig. 2. Dorsal cranial volume was measured in the region indicated by white outlines. **(A)** The dorsal aorta (DA) was chosen as the most ventral boundary, while the dorsal longitudinal vein (DLV) constituted the most dorsal. **(B)** Exclusion of unspecified regions, such as the eye (indicated with asterix) were excluded via manual ROI selection. Anterior and posterior inclusion were based on prosencephalic artery (PrA) and posterior cerebral vein (PCeV), while lateral inclusion was guided by the anatomy of primordial midbrain channel (PMBC).

Image Segmentation and Total Volume Measurement Intensity-based segmentation was performed to distinguish vascular from non-vascular tissue based on global Otsu thresholding [36] with morphological opening [37] and manual refinement where necessary.

Following segmentation, total dorsal cranial vascular volume (Vol [μm^3], Eq. 1) was calculated by multiplying the total count of vascular voxels in the region of interest (V_{vasc}, Fig. 2) by the respective voxel volume ($V_{x,y,z}$ [μm^3]).

$$Vol = V_{vasc} * V_{x,y,z} \tag{1}$$

Contrast-to-Noise Ratio (CNR) Data quality and variability across a range of vessel sizes was assessed using CNR measurements. Regions of interest (spanning the vascular cross-section, 5 μm length) were placed in candidate vessels at 3 dpf. Non-vascular (nv) measurements were taken from central regions of brain, without vascularization, at the same stack depth as the respective vessels. An estimate of background noise was obtained by measuring the standard deviation in a region of interest placed outside of the fish. CNR (Eq. 2) was calculated, as below:

$$CNR = \frac{\mu_v - \mu_{nv}}{\sigma} = \frac{mean\ signal - mean\ non\text{-}vascular\ signal}{standard\ deviation\ of\ background} \tag{2}$$

2.4 Statistics and Data Representation

Conformity of data to a Gaussian distribution was verified using D'Agostino-Pearson omnibus test [38]. Statistical analysis was performed using One-way

ANOVA or paired students t-test in GraphPad Prism Version 7 (GraphPad Software, La Jolla California USA). P values are represented using the following notation: $p < 0.05$ *, $p < 0.01$ **, $p < 0.001$ ***, $p < 0.0001$ ****. Graphical representations use mean values and standard deviation. Correlation analysis was performed with Pearson's correlation coefficient. Image representation and visualization was done with Inkscape Version 0.48 (https://www.inkscape.org).

3 Results and Discussion

3.1 Contrast-to-Noise Ratio in Developing Zebrafish Vasculature

To investigate the ability to reliably detect vascular structures, CNR was quantified in three different transgenic lines, which label different subcellular compartments as follows: membrane in *tg(kdrl:HRAS-mCherry)*^{s916} [22, 23], cytosol in *tg(fli1a:eGFP)*^{y1} [29] and filamentous actin in *tg(fli1a:Lifeact-mClover)*^{sh467} [30]. The vascular CNR was found to significantly differ between these transgenic lines (Fig. 3), which is likely to arise from differences in promotor and fluorophore constellation. Interestingly, non-vascular SNR, which arises mainly due to light scattering and autofluorescence, was fairly consistent in different transgenic lines.

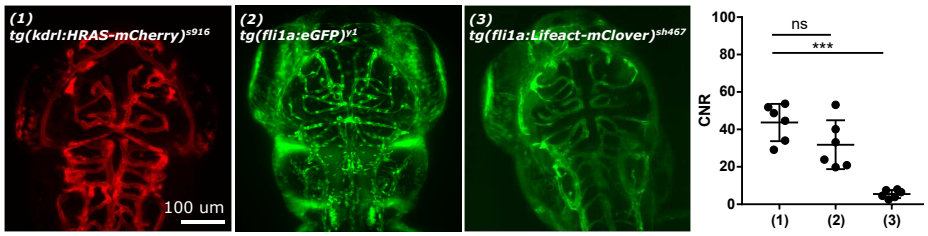

Fig. 3. The CNR in the basal artery was found to differ significantly between transgenic reporter lines, which can be used to visualize different subcellular components of vascular endothelial cells such as **(1)** membrane, **(2)** cytosol, **(3)** filamenteous actin (n = 6 embryos).

To, further, elucidate whether CNR is a function of vascular diameter the signal distribution of fluorescence in the dorsal cranial vasculature of transgenic lines (Fig. 4A) was measured in vessel segments of distinct anatomical locations (Fig. 4B) and diameters (Fig. 4C). As no significant difference between vessel CNR was found based on vascular diameter, we propose that contrast fluctuations were due to local and global transgenic reporter expression as well as image acquisition variations *per se*. Thus, vessels of varying size are expected to be segmented with a similar efficiency.

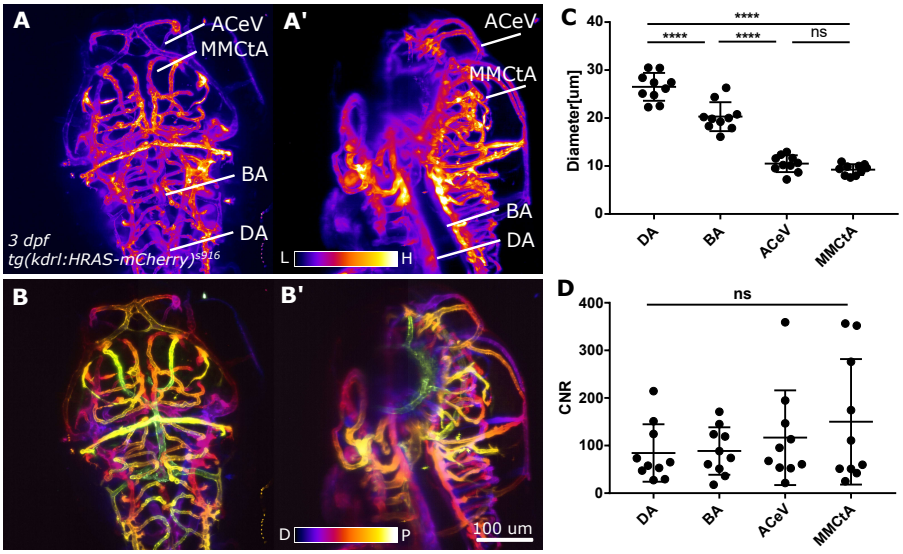

Fig. 4. (A, A') Maximum intensity projections of acquired dorsal and lateral 3D stacks show local variations of fluorescent reporter signal (Lookup table fire: L - low, H - high). **(B, B')** Colour-coded depth projection (lookup table fire: D - distal, P - proximal). **(C)** Diameters of analysed vessels. **(D)** CNR of respective vessels (n = 10 embryos). *Abbr.:* ACeV - anterior cerebral vein, BA - basilar artery, DA - dorsal aorta, MMCtA - middle mesencephalic central artery;

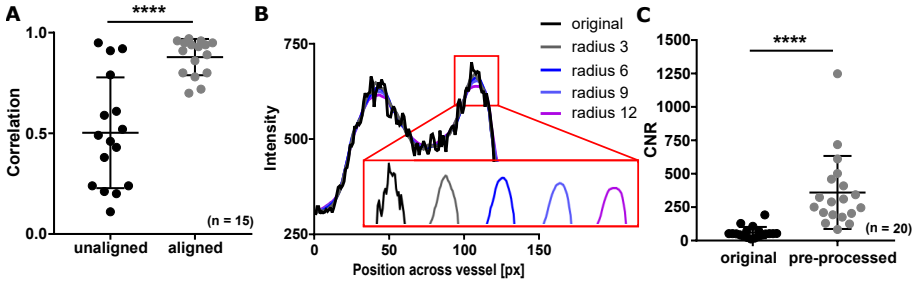

Fig. 5. (A) Correlation between first and last stack in 10 min time-lapse movies was significantly increased via applied motion correction. **(B)** Application of median filter with a 13-by-13 neighbourhood (blue line; radius 6) was found to reduce noise, whilst preserving vascular edge response (intensity measurement in BA cross-section; representative cross-section intensity distribution). **(C)** Image enhancement, including the removal of noise spikes and background, significantly increased the vascular CNR. (n numbers apply to individual embryos)

3.2 Data Pre-Processing to Restore and Enhance Data Quality

Motion artefacts were often observed to affect image analysis. Thus, to evaluate the existence and extent of short-term motion artefacts, 80 sec single-slice time-lapse acquisition was performed, which is the approximate time scale of a typical whole-stack multi-colour image acquisition. Linear stack alignment based on scale invariant features [39, 40] (implemented by Stephan Saalfeld as a Plugin in Fiji [33]) was applied and increased the Pearson's correlation between first and last image pre-alignment from 0.971 ± 0.01839 to 0.993 ± 0.001341 post-alignment. Similarly, in longer time-lapse movies of 10 min, we found a significant increase in the Pearson's correlation between first and last image pre-alignment: 0.5032 ± 0.2749, post-alignment: 0.8788 ± 0.0904 (Fig. 5A; p value < 0.0001).

For subsequent image segmentation and binarization, image acquisition artefacts were removed to enhance image quality, as follows. Application of 2D median filtering with a 13-by-13 neighbourhood was found to reduce image noise, while preserving vascular edge responses without blurring vascular walls (Fig. 5B) [34]. Large-scale image background was deducted by applying the rolling ball algorithm of size 200 as it was found to robustly reduce background noise [35]. The efficiency of image enhancement was evaluated via CNR measurement in the basilar artery (BA), which showed significant image enhancement as a result of the pre-processing (Fig. 5C; CNR vascular to pre-processed vascular p < 0.0001).

3.3 Vascular Segmentation

Classification into vascular and non-vascular voxels by segmentation was found to be achievable via intensity-based thresholding using the Otsu threshold [36] implemented in Fiji [33]. The pre-processing and segmentation pipeline delivered good results, upon visual inspection, in the transgenic line *tg(kdrl:HRAS-mCherry)*^{s916} [22, 23] (Fig. 6A). The sensitivity of total vascular volume measurements (Vol [μm^3], Eq. 1) to increasing levels of noise was evaluated and our proposed vasculature segmentation workflow showed high robustness over a wide range of noise levels (Fig. 6B; coefficient of variance between LP1.2% and LP0.4% 7.68%).

As expected, due to the differences in vascular signal profiles, some larger vessel volumes will be underestimated due to the drop off in signal towards the vessel centre. Future work will aim to overcome this limitation.

3.4 Summary

Our work so far has given insights into the signal distribution in vasculature-specific transgenic reporter lines of zebrafish. Moreover, we determined that vascular CNR is neither directly dependent on the anatomical location of vessel segments nor the diameter of tested candidate vessels. We propose that CNR variability is mainly caused by local fluorescent reporter variabilities or image-acquisition dependent alterations. We have shown that motion correction post-image acquisition is a necessity to restore the structural vascular integrity and

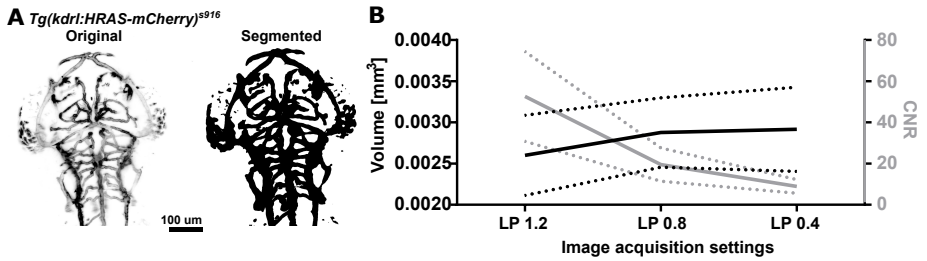

Fig. 6. (A) Intensity-based image binarization was found to efficiently segment the zebrafish vasculature the transgenic reporter lines *tg(kdrl:HRAS-mCherry)*^{s916} [22, 23]. **(B)** The total dorsal cranial vascular volume was measured in images with decreasing image quality (depicted by CNR levels) and was found to deliver robust results over a broad range of image qualities (4dpf *tg(kdrl:HRAS-mCherry)*^{s916} *[22, 23]; n = 10 larvae; mean: solid line, dotted line: standard deviation).*

can be achieved by linear stack alignment based on scale invariant features. Image pre-processing, via reduction of noise and background, increased the vascular CNR significantly, which simplified the application of image segmentation for subsequent image binarization. Herein, we have found that global intensity-based thresholding using the Otsu method [36] is able to distinguish vascular from non-vascular voxels in images acquired with LSFM of the developing cranial vasculature in zebrafish.

4 Future Perspectives

While the above proposed pre-processing and segmentation pipeline has provided a first step towards quantitative characterisation of the zebrafish vasculature, further refinement and optimisation is required. In particular, the segmentation methodology will be further investigated to clarify whether a 3D hole filling algorithm can overcome undersegmentation, which may arise in larger vessels due to the distinctive intensity distribution in transgenic zebrafish in comparison to images obtained with microangiography (Fig. 1).

Further, vascular centrelines will be extracted, according to requirements proposed in Cornea et al. [41]. Based on this simplified shape description 3D branching points, vessel segment length, diameter and curvature will be extracted. In addition, this modelling may overcome the limitations of straightforward segmentation methods described above, and reliably extract vascular volumes. Existing and novel algorithms shall be applied by implementation in the framework of open-source Software Fiji [33] to support distribution and development of analytical objectives under GNU General Public License.

Using 3D rigid image registration and hierarchical vessel classification will further help to elucidate vascular patterns, their changes during early cardiovascular development, and their alterations in disease. Hence, this work may help

to fully exploit the potential of zebrafish as a preclinical model of cardiovascular development and disease.

Acknowledgments: We thank the reviewers for critically reading and clarifying important aspects of the manuscript. This work was supported by a University of Sheffield, Department of Infection, Immunity and Cardiovascular Disease, Imaging and Modelling Node Studentship.

References

1. Gut, P., Reischauer, S., Stainier, D.Y.R., Arnaout, R.: Little Fish, Big Data: Zebrafish as a Model for Cardiovascular and Metabolic Disease. Physiological Reviews **97**(3) (July 2017) 889–938
2. Chico, T.J.A., Ingham, P.W., Crossman, D.C.: Modeling Cardiovascular Disease in the Zebrafish. Trends in Cardiovascular Medicine **18**(4) (May 2008) 150–155
3. Poole, T.J., Coffin, J.D.: Vasculogenesis and angiogenesis: two distinct morphogenetic mechanisms establish embryonic vascular pattern. The Journal of Experimental Zoology **251**(2) (August 1989) 224–231
4. Demir, R., Yaba, A., Huppertz, B.: Vasculogenesis and angiogenesis in the endometrium during menstrual cycle and implantation. Acta Histochemica **112**(3) (May 2010) 203–214
5. Adair, T.H., Montani, J.P.: Angiogenesis. Integrated Systems Physiology: from Molecule to Function to Disease. Morgan & Claypool Life Sciences, San Rafael (CA) (2010)
6. Carmeliet, P.: Angiogenesis in life, disease and medicine. Nature **438**(7070) (December 2005) 932–936
7. Carla, C., Daris, F., Cecilia, B., Francesca, B., Francesca, C., Paolo, F.: Angiogenesis in Head and Neck Cancer: A Review of the Literature. Journal of Oncology **2012** (2012)
8. Weinstein, B.M., Stemple, D.L., Driever, W., Fishman, M.C.: Gridlock, a localized heritable vascular patterning defect in the zebrafish. Nature Medicine **1**(11) (November 1995) 1143–1147
9. Schmitt, C.E., Holland, M.B., Jin, S.W.: Visualizing vascular networks in zebrafish: an introduction to microangiography. Methods in Molecular Biology (Clifton, N.J.) **843** (2012) 59–67
10. Lawson, N.D., Weinstein, B.M.: Arteries and veins: making a difference with zebrafish. Nature Reviews Genetics **3**(9) (September 2002) 674–682
11. Sydor, A.M., Czymmek, K.J., Puchner, E.M., Mennella, V.: Super-Resolution Microscopy: From Single Molecules to Supramolecular Assemblies. Trends in Cell Biology **25**(12) (December 2015) 730–748
12. Huisken, J., Swoger, J., Del Bene, F., Wittbrodt, J., Stelzer, E.H.K.: Optical sectioning deep inside live embryos by selective plane illumination microscopy. Science (New York, N.Y.) **305**(5686) (August 2004) 1007–1009
13. Santi, P.A.: Light sheet fluorescence microscopy: a review. The Journal of Histochemistry and Cytochemistry: Official Journal of the Histochemistry Society **59**(2) (February 2011) 129–138
14. Weber, M., Mickoleit, M., Huisken, J.: Light sheet microscopy. Methods in Cell Biology **123** (2014) 193–215
15. Stelzer, E.H.K.: Light-sheet fluorescence microscopy for quantitative biology. Nature Methods **12**(1) (January 2015) 23–26

16. Saleh, B.E.A., Teich, M.C.: Fundamentals of Photonics. 2 edn. John Wiley & Sons, Hoboken, N.J (April 2007)
17. Stelzer: Contrast, resolution, pixelation, dynamic range and signal-to-noise ratio: fundamental limits to resolution in fluorescence light microscopy. Journal of Microscopy **189**(1) (January 1998) 15–24
18. Watson, T.: Fact and Artefact in Confocal Microscopy. Advances in Dental Research **11**(4) (November 1997) 433–441
19. Hell, S., Reiner, G., Cremer, C., Stelzer, E.H.K.: Aberrations in confocal fluorescence microscopy induced by mismatches in refractive index. Journal of Microscopy **169**(3) (March 1993) 391–405
20. Power, R.M., Huisken, J.: A guide to light-sheet fluorescence microscopy for multiscale imaging. Nature Methods **14**(4) (March 2017) 360–373
21. Mikut, R., Dickmeis, T., Driever, W., Geurts, P., Hamprecht, F.A., Kausler, B.X., Ledesma-Carbayo, M.J., Mare, R., Mikula, K., Pantazis, P., Ronneberger, O., Santos, A., Stotzka, R., Strhle, U., Peyriras, N.: Automated Processing of Zebrafish Imaging Data: A Survey. Zebrafish **10**(3) (June 2013) 401–421
22. Chi, N.C., Shaw, R.M., De Val, S., Kang, G., Jan, L.Y., Black, B.L., Stainier, D.Y.: Foxn4 directly regulates tbx2b expression and atrioventricular canal formation. Genes & Development **22**(6) (March 2008) 734–739
23. Hogan, B.M., Bos, F.L., Bussmann, J., Witte, M., Chi, N.C., Duckers, H.J., Schulte-Merker, S.: Ccbe1 is required for embryonic lymphangiogenesis and venous sprouting. Nature Genetics **41**(4) (April 2009) 396–398
24. Feng, J., Cheng, S.H., Chan, P.K., Ip, H.H.S.: Reconstruction and representation of caudal vasculature of zebrafish embryo from confocal scanning laser fluorescence microscopic images. Computers in Biology and Medicine **35**(10) (December 2005) 915–931
25. Feng, J., Ip, H.H.S., Cheng, S.H., Chan, P.K.: A relational-tubular (ReTu) deformable model for vasculature quantification of zebrafish embryo from microangiography image series. Computerized Medical Imaging and Graphics: The Official Journal of the Computerized Medical Imaging Society **28**(6) (September 2004) 333–344
26. Feng, J., Ip, H.H.S.: A statistical assembled deformable model (SAMTUS) for vasculature reconstruction. Computers in Biology and Medicine **39**(6) (June 2009) 489–500
27. Chen, Q., Jiang, L., Li, C., Hu, D., Bu, J.w., Cai, D., Du, J.l.: Haemodynamics-Driven Developmental Pruning of Brain Vasculature in Zebrafish. PLOS Biology (2012)
28. Pries, A.R., Cornelissen, A.J.M., Sloot, A.A., Hinkeldey, M., Dreher, M.R., Hpfner, M., Dewhirst, M.W., Secomb, T.W.: Structural Adaptation and Heterogeneity of Normal and Tumor Microvascular Networks. PLOS Computational Biology **5**(5) (May 2009) e1000394
29. Lawson, N.D., Weinstein, B.M.: In Vivo Imaging of Embryonic Vascular Development Using Transgenic Zebrafish. Developmental Biology **248**(2) (August 2002) 307–318
30. Savage, A.M., Mayo, C., Kim, H.R., Markham, E., Eeden, F.J.M.v., Chico, T.J.A., Wilkinson, R.N.: Generation and characterisation of novel transgenic zebrafish allowing in vivo imaging of endothelial cell biology. Atherosclerosis **244** (January 2016) e10
31. Westerfield, M.: The Zebrafish Book: A Guide for Laboratory use of Zebrafish (Brachydanio rerio). 2nd edition edn. University of Oregon Press (1993)

32. Kimmel, C.B., Ballard, W.W., Kimmel, S.R., Ullmann, B., Schilling, T.F.: Stages of embryonic development of the zebrafish. Developmental Dynamics **203**(3) (1995) 253–310
33. Schindelin, J., Arganda-Carreras, I., Frise, E., Kaynig, V., Longair, M., Pietzsch, T., Preibisch, S., Rueden, C., Saalfeld, S., Schmid, B., Tinevez, J.Y., White, D.J., Hartenstein, V., Eliceiri, K., Tomancak, P., Cardona, A.: Fiji - an Open Source platform for biological image analysis. Nature methods **9**(7) (June 2012)
34. Lim, J.: Two-Dimensional Signal and Image Processing. Englewood Cliffs, NJ, Prentice Hall (1990) 469–476
35. Sternberg, S.: Biomedical Image Processing. Computer **16** (1983) 22–34
36. Otsu, N.: A threshold selection method from gray-level histograms. Trans. Sys.Man. **9**(1) (1979) 62–66
37. Serra, J.: Image Analysis and Mathematical Morphology. Academic Press, Inc., Orlando, FL, USA (1983)
38. D'Agostino, R.B., Belanger, A.: A Suggestion for Using Powerful and Informative Tests of Normality. The American Statistician **44**(4) (1990) 316–321
39. Lowe, D.: Object Recognition from Local Scale-Invariant Features. In: Proc. of the International Conference on Computer Vision, Corfu (1999)
40. Lowe, D.G.: Distinctive Image Features from Scale-Invariant Keypoints. International Journal of Computer Vision **60**(2) (November 2004) 91–110
41. Cornea, N., Min, P., Silver, D.: Curve-skeleton properties, applications, and algorithms. IEEE Transactions on Visualization and Computer Graphics **13**(3) (2007) 530–548